Physica A 464 (2016) 93–102

Contents lists available at ScienceDirect

Physica A

journal homepage: www.elsevier.com/locate/physa

Time series characterization via horizontal visibility graph and Information Theory

Bruna Amin Gonçalves [a], Laura Carpi [b], Osvaldo A. Rosso [c,d,e], Martín G. Ravetti [a,*]

[a] Departmento de Engenharia de Produção, Universidade Federal de Minas Gerais, 31270-901, Belo Horizonte, MG, Brazil

[b] Departament de Física i Enginyeria Nuclear, Universitat Politècnica de Catalunya, 08222 Terrassa, Spain

[c] Departmento de Física, Universidade Federal de Alagoas, 57072-970, Maceió, AL, Brazil

[d] Instituto Tecnológico de Buenos Aires (ITBA), CONICET, C1106ACD, Ciudad Autónoma de Buenos Aires, Argentina

[e] Complex Systems Group, Facultad de Ingeniería y Ciencias Aplicadas, Universidad de los Andes, Las Condes, Santiago, Chile

HIGHLIGHTS

- This work deals with the characterization of dynamical systems using Horizontal Visibility Graphs (HVG) and Information Theory quantifiers.
- We propose the use of the weight distribution, which is based on the difference of the time series values of connected points.
- We study fractional Brownian motion time series and a paleoclimatic proxy record of ENSO taken from Pallcacocha Lake.
- The weight distribution allows a better characterization of the studied systems, using considerable shorter time series.

ARTICLE INFO

Article history:
Received 8 March 2016
Received in revised form 27 May 2016
Available online 29 July 2016

Keywords:
Time series analysis
Complex networks
Information Theory quantifiers

ABSTRACT

Complex networks theory have gained wider applicability since methods for transformation of time series to networks were proposed and successfully tested. In the last few years, horizontal visibility graph has become a popular method due to its simplicity and good results when applied to natural and artificially generated data. In this work, we explore different ways of extracting information from the network constructed from the horizontal visibility graph and evaluated by Information Theory quantifiers. Most works use the degree distribution of the network, however, we found alternative probability distributions, more efficient than the degree distribution in characterizing dynamical systems. In particular, we find that, when using distributions based on distances and amplitude values, significant shorter time series are required. We analyze fractional Brownian motion time series, and a paleoclimatic proxy record of ENSO from the Pallcacocha Lake to study dynamical changes during the Holocene.

1. Introduction

In the last few years, methods to transform time series into networks have been proposed, and with them, novel ways to analyze and characterize time series, have been developed. Among others, these novel methodologies include the use of disjoint cycles and their distances in the phase space to generate the links in the corresponding network [1,2]. Li and Wang

* Corresponding author.
E-mail address: martin.ravetti@dep.ufmg.br (M.G. Ravetti).

http://dx.doi.org/10.1016/j.physa.2016.07.063
0378-4371/

[3,4] introduce a method based on n-tuples. Donner et al. [5,6] work with recurrence networks. There are also methods based on the phase space reconstruction of the time series [2,7,8]. Latora et al. [9] propose a graph based on the recurrence of time series motifs. Other methods take into account the visibility of elements in a time series, like the Visibility Graphs or the Horizontal Visibility Graphs [10,11]. Our article focuses on the use of the latter.

Following previous works [12,13], we extract probability distribution functions (PDFs) from the constructed networks to characterize the topological structure and to capture the dynamics of the transformed time series, using Information Theory quantifiers. Related works have primarily focused on the network's degree distribution. We investigate in this work, alternative probability distributions and we compare their performance with the usual degree distribution. Specifically, we explore the distance distribution, that despite being poorly explored, it was shown to be efficient in capturing network's topological changes [14]. We also propose a PDF based on the difference of the time series values (amplitudes) between the nodes connected by the horizontal visibility algorithm. We find the distance distribution and the one based on amplitude differences more efficient in characterizing the studied systems as they require significantly shorter time series than the degree distribution.

We study fractional Brownian motion (fBm) time series generated with different degrees of correlations (different Hurst exponents), and a paleoclimatic proxy record of the Laguna Pallcacocha used to study the millennial El Niño/Southern Oscillation (ENSO) dynamic.

2. Horizontal visibility graph and associated PDFs

The horizontal visibility graph (HVG) is a methodology that transforms a time series into a graph maintaining the inherent characteristics of the transformed time series [11]. The HVG consists in a geometrical simplification of the firstly proposed visibility graph (VG) [10]. It considers each point in the time series, a node in the network, connected by the following consideration: Let $\{x_i,\ i = 1, \ldots, N\}$, be a time series of N data. Two nodes i and j in the graph are connected if it is possible to trace a horizontal line, in the time series, linking x_i and x_j not intersecting intermediate data height, fulfilling: $x_i,\ x_j > x_n$ for all $i < n < j$.

In the HVG, the nodes can see at least its nearest neighbors, incorporating in a natural way the time causality. One of the properties of the HVG is that it is not modified under rescaling of horizontal and vertical axes, as well as under horizontal and vertical translations [11,15].

2.1. Probability distributions extracted from HVG

Once the graph is constructed, several ways of extracting information about its structure are possible. The most usual one is to extract the degree distribution that describes the way the node's degrees are distributed in the graph. The degree distribution has been used to study several natural and artificial systems, from river flows [16], to laser intensity analysis [17]. For a given network G with N nodes, the degree distribution, $P_{deg}(\kappa)$, is the fraction of nodes with degree κ. This discrete distribution is defined on the set $\{0, 1, \ldots, N-1\}$.

Other probability distributions, such as the distance distribution have been still poorly explored, however, one recent work has shown the distance distribution to be very effective in capturing network's topological changes [14]. The distance between a pair of nodes is the shortest path between them, thus, the distance distribution, $P_\delta(d)$, is the fraction of pairs of nodes at distance d. The maximum possible distance is $N-1$, and when a pair is disconnected, we consider ∞, thus, the distance distribution is discrete and defined over the set $\{1, 2, \ldots, N-1, \infty\}$.

In this article, we also explore a straightforward modification of HVG, that consists in weighting the edges based on the difference between two connected values in the time series. The weight of an edge is a real value proportional to the amplitude difference between two connected points. Considering $\mathbf{x} = \{x_1, \ldots, x_n\}$ a sample of n real values, if x_i and x_j are connected, the edge (i, j) has a weight $w_{ij} = x_i - x_j$. It is important noticing that, if we keep track of the first value of the time series, we could reconstruct the series from the resulting graph. As w_{ij} is a continuous variable, a histogram is constructed to estimate the probability distribution. $P_w(A)$ represents the fraction of edges with amplitude A. Fig. 1 exemplifies how these PDFs are obtained from a time series.

3. Information theory quantifiers

3.1. Shannon entropy

When considering discrete probability distributions ($P = \{p_j : j = 1, \ldots, M\}$) the *Shannon entropy* $S[P]$ [18] is defined as:

$$S[P] = -\sum_{j=1}^{M} p_j \cdot \ln p_j. \tag{1}$$

If $S[P] = 0$ we are in a position to predict with certainty *which* of the possible outcomes j whose probabilities are given by p_j will actually take place. Our knowledge of the underlying process described by the probability distribution is, in this

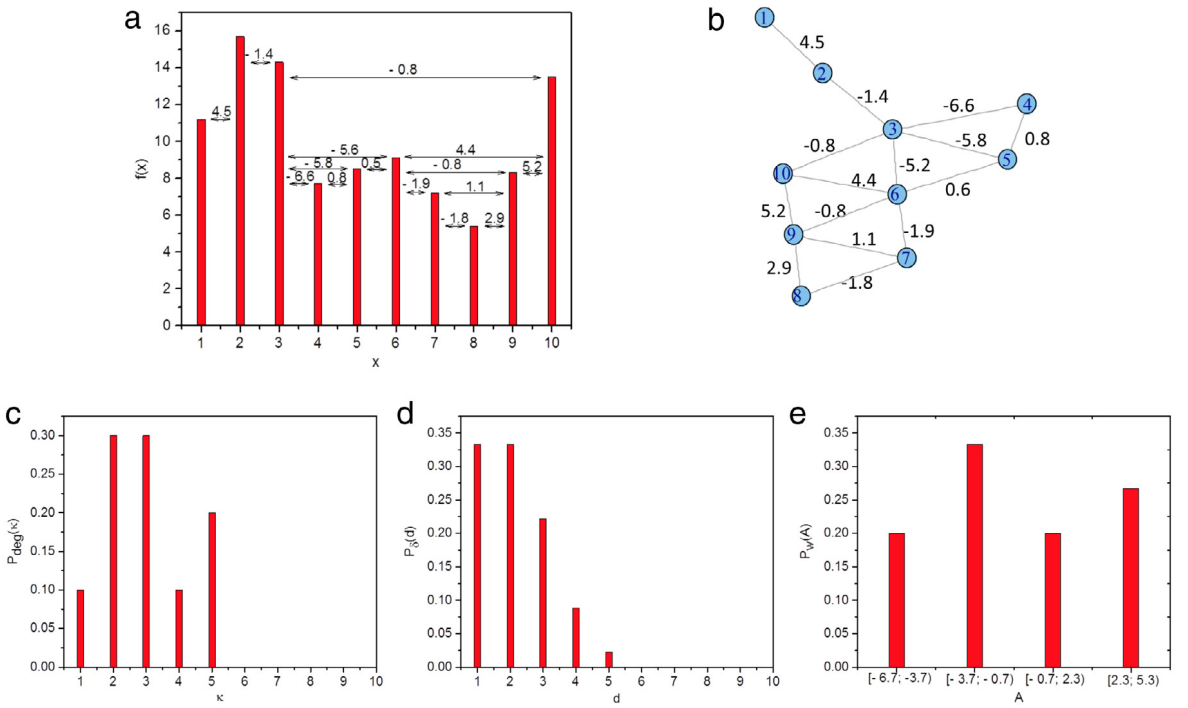

Fig. 1. Example of the transformation of a time series into a graph (HVG), and the three different probabilities distributions extracted from it. Subfigure (a) shows the time series, (b) depicts the network after applying HVG, the weights are only considered for P_w, (c) degree distribution P_{deg} (d) distance distribution P_δ and (e) weight distribution P_w.

instance, maximal. On the contrary, our ignorance is maximal for a uniform distribution. For a given distribution P, the "normalized Shannon entropy" is computed as $S[P]/S_{\max}$. For the cases here analyzed, $S_{\max} = \ln(M)$, where $M = N$ for P_{deg} and P_δ and M is equal to the number of bins of the histogram for P_w. The Shannon entropy presents a global perspective of the density, as it is not sensitive to permutations of its bins, however, it will detect changes in their values.

3.2. Fisher's Information Measure

The *Fisher's Information Measure* (F) constitutes a measure of the gradient content of the distribution, being quite sensitive even to small localized perturbations [19,20]. Considering the same probability distribution P, it reads as:

$$F[P] = F_0 \sum_{i=1}^{M-1} [(p_{i+1})^{1/2} - (p_i)^{1/2}]^2. \tag{2}$$

It has been extensively discussed that this discretization is the best behaved in a discrete environment [21]. Here, the normalization constant F_0 reads

$$F_0 = \begin{cases} 1 & \text{if } p_{i^*} = 1 \text{ for } i^* = 1 \text{ or } i^* = M \text{ and } p_i = 0\ \forall i \neq i^* \\ 1/2 & \text{otherwise.} \end{cases} \tag{3}$$

3.3. Shannon–Fisher information plane

The use of the Shannon–Fisher information plane $S \times F$, was initially proposed by Vignat and Bercher [22] and later applied in several works [23–25]. In this plane, axes are functional of the probability density considered, the normalized Shannon Entropy ($S/S_{\max}$) and the Fisher Information measure F. The $S \times F$-plane is a suitable tool to contrast global and local features of the probability distribution under study.

4. Computational experiments

4.1. Characterization of fBm

The first experiment evaluates the performance of the methodology over artificially created time series. We study fractional Brownian motion (fBm) time series, that are continuous-time Gaussian processes, self-similar, and endowed with

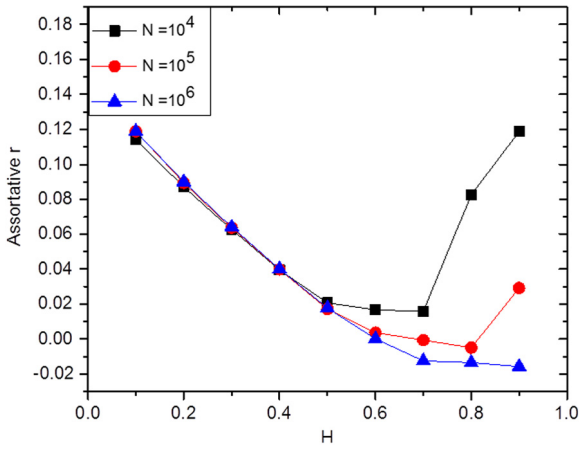

Fig. 2. Average results for fBm with different Hurst exponent values and lengths. Each value is the average result of 30 independent runs.

stationary increments [26]. Motion and noise are characterized by the Hurst exponent (H), that describes the raggedness of the motion. The Hurst's parameter defines two distinct regions in the interval $(0, 1)$. For $H > 1/2$, consecutive increments tend to have the same sign, thus, these processes are *persistent*. On the contrary, for $H < 1/2$, consecutive increments are more likely to have opposite signs, being *anti-persistent*. The case $H = 1/2$ corresponds to the classical Brownian motion, where successive motion increments are as likely to have the same sign as the opposite, presenting no correlation among them. We generate the fBm time series with Hurst exponent in the range $0.1 \leq H \leq 0.9$ of different lengths with the algorithm proposed by Abry and Sellan [27,28], by using its Matlab implementation.

A few works devoted to the study of the characterization of fBm uses HVG related methodologies [11,15,23,29–31]. Lacasa et al. [29] show that the degree distribution of the network constructed from fBm time series is a function of the Hurst exponent. In Ravetti et al. [23] the Fisher–Shannon information plane is used to discriminate different degrees of correlations in fBm by considering the HVG degrees distributions.

In a recent publication, [15], an analysis is performed on HVG and network features by considering fBm processes. They use time series length of 10^4 and they correlate common network features with the Hurst exponent. One curious result is that the assortativity coefficient[1] decreases until reaching a turning point around $H = 0.6$. We reproduced the experiment performed in the above-mentioned article, finding similar results regarding the relation between the networks quantifiers via HVG and the fBm, with the exception of the assortativity coefficient. The phase transition claimed by the authors at $H = 0.6$ is not real, but a consequence of the time series length. The use of HVG and the computation of network features for the analysis of fBm time series for $H > 0.6$ require time series larger than 10^4 to be accurate, as shown in Fig. 2. Additional results are described in the Supplementary Information (SI), see Figure S1.

The use of Information Theory with the HVG shows remarkable results. The HVG is capable of capturing the increasing persistence of the series with increasing values of H. Results are depicted in Fig. 3. In the subfigures, each graph illustrates a sample of the HVG outcome for each Hurst exponent value. It is possible to visually notice how the persistence of the series is captured by the HVG and reflected by network features.

Regarding the time series characterization, the three probability densities are able to discriminate all series of a length of 10^5 in the $S \times F$-plane. When considering the degree distribution, the highest point in the plane corresponds to the time series with lower values of H, with $H = 0.1$ presenting the highest values of Fisher and Shannon entropies. As correlation increases, the time series begin to present longer sequences with increasing and/or decreasing values, generating bigger valleys and increasing the visibility of certain points. The networks begin to reflect that effect by increasing the degree of a small group of nodes. The degree densities present a decrease of peaks, but at the same time, their tails get shorter, moving apart from the uniform distribution, thus, the entropy values diminish, see Fig. 4(a). It is important mentioning that the Fisher Information Measure (F) is unable to discriminate time series with higher H values with this series length. However, results considering time series with a length of 10^6 show an improved performance of F, see SI Figure S3. These results are consistent with findings discussed in Ref. [23].

When considering the distance distribution, the locations in the plane change. Small values of H indicate shorter path lengths (L), the visibility of two points in the time series will be interrupted depending on the correlation level, no correlation will generate interruptions at an almost regular pace. This structure generates shortcuts between the nodes reducing the path between them. As H increases, the interruption may happen right away, increasing the number of nodes between the two points and increasing L (see SI Figure S1).

[1] Also known as the Pearson correlation coefficient.

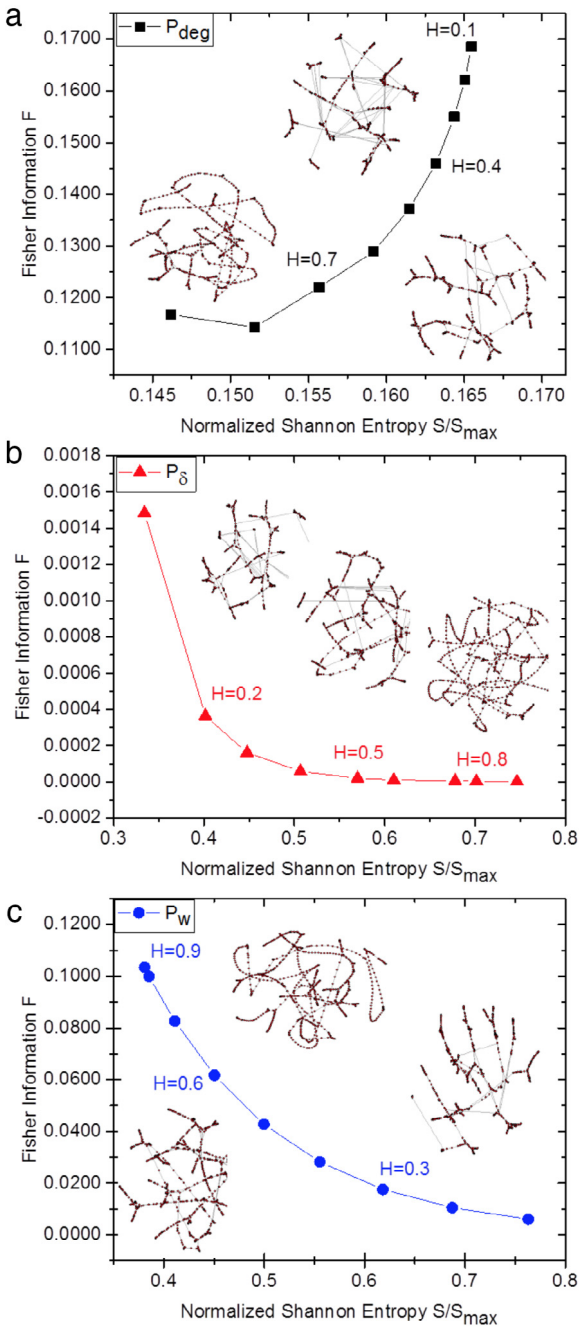

Fig. 3. Shannon–Fisher plane for each probability density. In each case the average results over 10 independent runs for fBm with different Hurst exponent values are presented considering a time series length of 10^5 points. Subfigure (a) considers the degree distribution. Subfigure (b) uses the distance distribution and (c) the weighted density. The graphs in the figures are subplots of HVG results.

The increase of H causes the distance densities to get closer to the uniform distribution and the Shannon entropy values get higher, see Fig. 4(b). In the case of F, the measurement is much more sensitive to small localized perturbations. Differently from the degree distribution, more changes happen in the different states of the distance distribution, increasing the value of F.

In the case of the weight distribution P_w, for smaller values of H the amplitude differences are higher and the PDFs present longer tails being closer to the uniform distribution, see Fig. 4(c). As the H value increases, the absolute value of the amplitude's differences is smaller, consequently, the central bins increase their frequency, tails get shorter and the Shannon entropy value decreases. From Fig. 4(c), it is possible to see that as H increases greater perturbations happen near the central bins, increasing in this way the value of F.

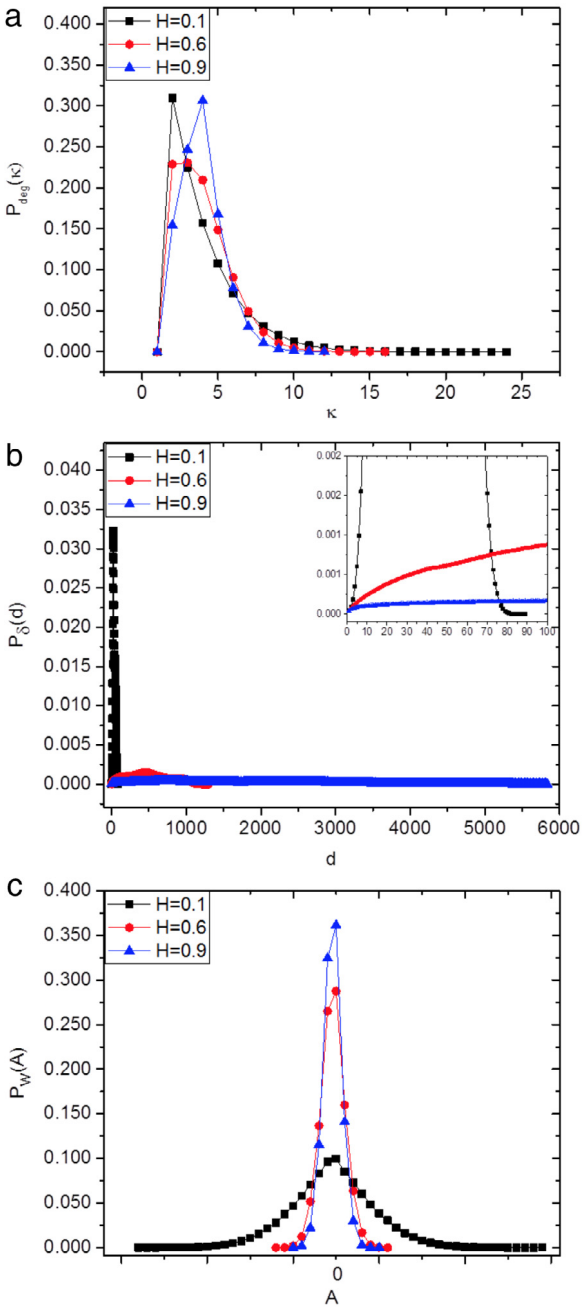

Fig. 4. Probability distributions extracted from the graph for different values of the Hurst exponent. Subfigure (a) depicts how the degree distribution changes as H increases P_{deg}, (b) depicts the case for the distance distribution P_δ, and (c) for the weight distribution P_w.

It is noticeable how P_w is capable of smoothly capturing the dynamical changes of the time series, even needing less amount of data. Fig. 5, shows the same characterization considering time series with lengths 10^3. The Figure depicts the power of the HVG combined with the $S \times F$-plane and P_w. For length 10^4 see Figure S2 in SI.

4.2. Millennial dynamics of El Niño Southern Oscillation

The second experiment is devoted to the evaluation of the three proposed probability distributions to study the variability of the El Niño-Southern Oscillation during the Holocene (ENSO) (11,000 years BP to present), by using a proxy record of ENSO from the Pallcacocha Lake sedimentary data [32,33]. The data used in this experiment was obtained through the analysis of clastic laminae deposition in two 8-m sediment cores retrieved from the Pallcacocha Lake in Ecuador, in which the

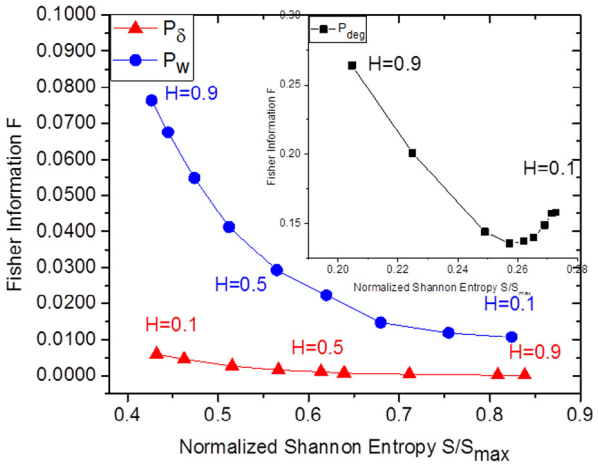

Fig. 5. Shannon-and-Fisher plane for each probability density. In each case the average results over 10 independent runs for fBm with different Hurst exponent values are presented considering a time series length of 10^3 points.

light-colored inorganic clastic sediments laminae are known to be correlated with moderate to severe El Niño events [32,34]. The time series is constructed from the red color intensity surface of the cores sections, that were digitally scanned. Then, it was applied an age model based on radiocarbon chronology [35]. Previous works using this data found evidence of long-range correlations extending to timescales of half a millennium [36], a cyclic behavior of approximately 2000 years, and a shift in variance around 5000 BP [32,34]. These works use wavelet analysis [32], ordinal analysis and Information Theory [34] and non-linear dynamic techniques [37].

In this work, the original time series [33] has been interpolated using a cubic Hermite polynomial to a one-year sample, as in Ref. [34]. HVG is constructed from temporal windows of 1000 years, lagged by 100 years. Then, Shannon entropy and Fisher information are computed for all windows. Fig. 6 shows the outcomes using the degree distribution (a), distance distribution (b), and the weight distribution (c). From these figures, it can be observed that the weight distribution detects, with a more pronounce and smooth behavior, a change in the ENSO dynamic around 5000 BP, moment in which the Shannon entropy finishes a long period of an increasing trend (the opposite occurs with Fisher Information).

It is also possible to see that the weight distribution better detects a period from around 9200 to 7500 of the early Holocene (a period that includes the first mayor Rapid Climate Change (RCC)[2] [37,38]), characterized by a steady behavior with low entropy values suggesting the presence of more correlated dynamics. This fact can also be seen in Fig. 7, as this period can be found where more correlated processes are located (see also Fig. 3(c)). This period is also identified in Ref. [34].

The weight distribution clearly points out to the existence of cycles with a period close to 2000 years during the mid-to-late Holocene. These findings are consistent with that observed by Moy et al. [32] using wavelet analysis, and Saco et al. [34] using ordinal patterns. This behavior is not captured by Shannon entropy and Fisher information when using HVG computed with the distance distribution. When using the degree distribution, the cyclic behavior is captured by both quantifiers, however, it is not as clear and smooth. The weight distribution shows to be more sensitive to dynamical changes than the other distributions. This result confirms that the weight distribution works better than the degree and distance distributions with shorter time series, detecting in this case, well-known ENSO features.

5. Discussion and conclusions

In this work, we analyze the performance of a methodology that combines Horizontal Visibility Graph and Information Theory quantifiers to characterize dynamical systems. Most works rely on the use of the HVG degree distribution, however, we show through extensive experimentation, that the weight distribution based on amplitude differences, allows a better characterization with considerable shorter time series, relevant fact when analyzing real systems. Persistent processes usually require very long time series to be properly characterized, and this fact has caused some confusion, specifically in the analysis of some networks features, such as the assortativity coefficient.

We study here, fractional Brownian motion generated time series with different degrees of correlations and dynamical changes of the El Niño-Southern Oscillation during the Holocene. In both cases, the weight distribution shows a better performance than the degree and distance distributions, properly distinguishing different degrees of correlations in fBm time series, and better characterizing the ENSO dynamic.

[2] RCC periods were identified by Denton and Karlén [38]. These periods have been frequently used as a framework for the examination of Holocene climate variability.

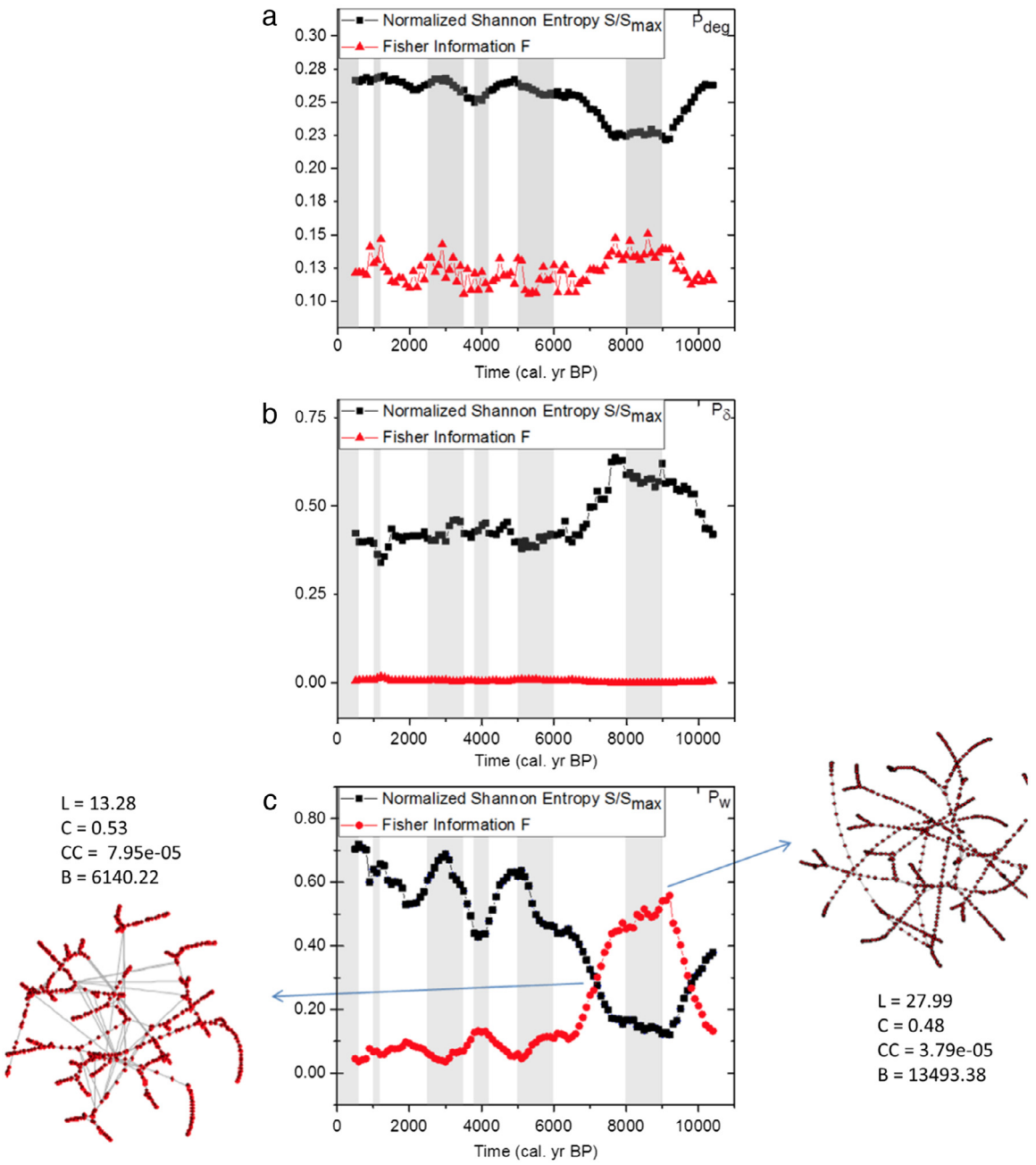

Fig. 6. Shannon entropy (black) and Fisher Information (red) values computed from HVG through (a) degree distribution, (b) distance distribution, and (c) weights distribution. For each depicted graph, *L* indicates the average path length, *CC* Closeness centrality, *C* Clustering coefficient and *B* Betweenness centrality. The gray bands correspond to RCC during the Holocene [37]. (For interpretation of the references to color in this figure legend, the reader is referred to the web version of this article.)

In summary, we propose an alternative way to extract information from the HVGs based on amplitude differences, and we demonstrate the higher efficiency in characterizing dynamical systems when compared to more commonly used techniques.

Acknowledgments

This research has been partially supported by CNPq and FAPEMIG. O.A. Rosso acknowledges partial support from the *Consejo Nacional de Investigaciones Científicas y Técnicas* (CONICET), Argentina.

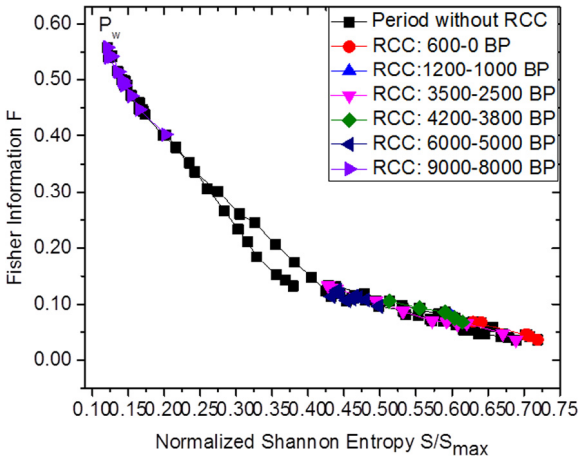

Fig. 7. Shannon entropy and Fisher Information values computed from HVG and located in the Shannon–Fisher plane. Colored points correspond to RCC during the Holocene [37]. (For interpretation of the references to color in this figure legend, the reader is referred to the web version of this article.)

Appendix A. Supplementary data

Supplementary material related to this article can be found online at http://dx.doi.org/10.1016/j.physa.2016.07.063.

References

[1] J. Zhang, M. Small, Complex network from pseudoperiodic time series: Topology versus dynamics, Phys. Rev. Lett. 96 (2006) 238701.
[2] X. Xu, J. Zhang, M. Small, Superfamily phenomena and motifs of networks induced from time series, Proc. Natl. Acad. Sci. 105 (50) (2008) 19601–19605.
[3] P. Li, B. Wang, An approach to Hang Seng index in Hong Kong stock market based on network topological statistics, Chinese Sci. Bull. 51 (5) (2006) 624–629.
[4] P. Li, B.-H. Wang, Extracting hidden fluctuation patterns of Hang Seng stock index from network topologies, Physica A 378 (2) (2007) 519–526.
[5] R.V. Donner, Y. Zou, J.F. Donges, N. Marwan, J. Kurths, Recurrence networks—a novel paradigm for nonlinear time series analysis, New J. Phys. 12 (3) (2010) 033025.
[6] R.V. Donner, M. Small, J.f. Donges, N. Marwan, Y. Zou, R. Xiang, J. Kurths, Recurrence-based time series analysis by means of complex network methods, Int. J. Bifurcation Chaos 21 (04) (2011) 1019–1046.
[7] Z. Gao, N. Jin, Complex network from time series based on phase space reconstruction, Chaos 19 (3) (2009) 033137.
[8] C. Liu, W.-X. Zhou, Superfamily classification of nonstationary time series based on DFA scaling exponents, J. Phys. A 43 (49) (2010) 495005.
[9] R. Sinatra, D. Condorelli, V. Latora, Networks of motifs from sequences of symbols, Phys. Rev. Lett. 105 (2010) 178702.
[10] L. Lacasa, B. Luque, F. Ballesteros, J. Luque, J.C. Nuño, From time series to complex networks: The visibility graph, Proc. Natl. Acad. Sci. 105 (13) (2008) 4972–4975.
[11] B. Luque, L. Lacasa, F. Ballesteros, J. Luque, Horizontal visibility graphs: Exact results for random time series, Phys. Rev. E 80 (4) (2009) 046103.
[12] L.C. Carpi, O.A. Rosso, P.M. Saco, M.G. Ravetti, Analyzing complex networks evolution through information theory quantifiers, Phys. Lett. A 375 (4) (2011) 801–804.
[13] L.C. Carpi, P.M. Saco, O. Rosso, M.G. Ravetti, Structural evolution of the tropical pacific climate network, Eur. Phys. J. B 85 (11) (2012) 1–7.
[14] T.A. Schieber, L. Carpi, A.C. Frery, O.A. Rosso, P.M. Pardalos, M.G. Ravetti, Information theory perspective on network robustness, Phys. Lett. A 380 (3) (2016) 359–364.
[15] W.-J. Xie, W.-X. Zhou, Horizontal visibility graphs transformed from fractional brownian motions: Topological properties versus the Hurst index, Physica A 390 (20) (2011) 3592–3601.
[16] A.C. Braga, L.G.A. Alves, L.S. Costa, A.A. Ribeiro, M.M.A. de Jesus, A.A. Tateishi, H.V. Ribeiro, Characterization of river flow fluctuations via horizontal visibility graphs, Physica A 444 (2016) 1003–1011.
[17] A. Aragoneses, L. Carpi, N. Tarasov, D.V. Churkin, M.C. Torrent, C. Masoller, S.K. Turitsyn, Unveiling temporal correlations characteristic of a phase transition in the output intensity of a fiber laser, Phys. Rev. Lett. 116 (2016) 033902.
[18] C.E. Shannon, A mathematical theory of communication, Bell Syst. Tech. J. 27 (3) (1948) 379–423.
[19] R. Fisher, On the mathematical foundations of theoretical statistics, Philos. Trans. R. Soc. Lond. Ser. A 222 (1922) 309–368.
[20] B. Frieden, Science from Fisher Information: A Unification, Cambridge University Press, 2004.
[21] P. Sánchez-Moreno, R. Yáñez, J. Dehesa, Discrete densities and Fisher information, in: Proceedings of the 14th International Conference on Difference Equations and Applications, Bahçeşehir University Press, 2009, pp. 291–298.
[22] C. Vignat, J. Bercher, Analysis of signals in the Fisher–Shannon information plane, Phys. Lett. A 312 (2003) 27–33.
[23] M.G. Ravetti, L.C. Carpi, B.A. Gonçalves, A.C. Frery, O.A. Rosso, Distinguishing noise from chaos: Objective versus subjective criteria using horizontal visibility graph, PLoS One 9 (9) (2014) e108004.
[24] O.A. Rosso, F. Olivares, L. Zunino, L. De Micco, A. Aquino, A. Plastino, H. Larrondo, Characterization of chaotic maps using the permutation Bandt-Pompe probability distribution, Eur. Phys. J. B 86 (2013) 116–129.
[25] F. Olivares, A. Plastino, O.A. Rosso, Contrasting chaos with noise via local versus global information quantifiers, Phys. Lett. A 376 (2012) 1577–1583.
[26] L. Zunino, D.G. Pérez, M.T. Martín, A. Plastino, M. Garavaglia, O.A. Rosso, Characterization of Gaussian self-similar stochastic processes using wavelet-based informational tools, Phys. Rev. E 75 (2) (2007) 021115.
[27] P. Abry, F. Sellan, The wavelet-based synthesis for fractional brownian motion proposed by F. Sellan and Y. Meyer: Remarks and fast implementation, Appl. Comput. Harmon. Anal. 3 (4) (1996) 377–383.
[28] J. Bardet, G. Lang, G. Oppenheim, A. Philippe, S. Stoev, M. Taqqu, P. Doukhan, M. Taqqu, Generators of Long-Range Dependence Processes: A Survey, Birkhauser, New York, 2003, pp. 579–623.
[29] L. Lacasa, B. Luque, J. Luque, J. Nuno, The visibility graph: A new method for estimating the Hurst exponent of fractional Brownian motion, Europhys. Lett. 86 (3) (2009) 30001.
[30] L. Lacasa, R. Toral, Description of stochastic and chaotic series using visibility graphs, Phys. Rev. E 82 (3) (2010) 036120.

[31] Y.H. , M. Stephen, C. Gu, Visibility graph based time series analysis, PLoS One 10 (11) (2015) e0143015.
[32] C.M. Moy, G.O. Seltzer, D.T. Rodbell, D.M. Anderson, Variability of El Nino/Southern Oscillation activity at millennial timescales during the holocene epoch, Nature 420 (6912) (2002) 162–165.
[33] C.M. Moy, G.O. Seltzer, D.T. Rodbell, D.M. Anderson, Laguna pallcacocha sediment color intensity data IGBP pages/world data center for paleoclimatology, data contribution series #2002-76 NOAA/NCDC Paleoclimatology Program Boulder CO, USA.
[34] P.M. Saco, L.C. Carpi, A. Figliola, E. Serrano, O.A. Rosso, Entropy analysis of the dynamics of El Niño/Southern Oscillation during the holocene, Physica A 389 (21) (2010) 5022–5027.
[35] D.T. Rodbell, G.O. Seltzer, D.M. Anderson, M.B. Abbott, D.B. Enfield, J.H. Newman, An ∼15,000-year record of El Niño-driven alluviation in southwestern ecuador, Science 283 (5401) (1999) 516–520.
[36] G. Wang, A.A. Tsonis, On the variability of ENSO at millennial timescales, Geophys. Res. Lett. 35 (17) (2008) L17702.
[37] A. Tsonis, Dynamical changes in the ENSO system in the last 11,000 years, Clim. Dynam. 33 (7–8) (2009) 1069–1074.
[38] G.H. Denton, W. Karlén, Holocene climatic variations—their pattern and possible cause, Quat. Res. 3 (2) (1973) 155–205.

Time Series Characterization via Horizontal Visibility Graph and Information Theory
Supplementary Material

Bruna Amin[a], Laura Carpi[b], Osvaldo A. Rosso[c,d,e], Martín G. Ravetti[a]

[a] *Departmento de Engenharia de Produção, Universidade Federal de Minas Gerais, 31270-901, Belo Horizonte, MG, Brazil*
[b] *Departament de Física i Enginyeria Nuclear, Universitat Politècnica de Catalunya, 08222 Terrassa, Spain*
[c] *Departmento de Física, Universidade Federal de Alagoas, 57072-970, Maceió, AL, Brazil*
[d] *Instituto Tecnológico de Buenos Aires (ITBA), CONICET, C1106ACD, Ciudad Autónoma de Buenos Aires, Argentina*
[e] *Complex Systems Group, Facultad de Ingeniería y Ciencias Aplicadas, Universidad de los Andes, Las Condes, Santiago, Chile.*

Email address: martin.ravetti@dep.ufmg.br (Martín G. Ravetti)

S1. Network feature results

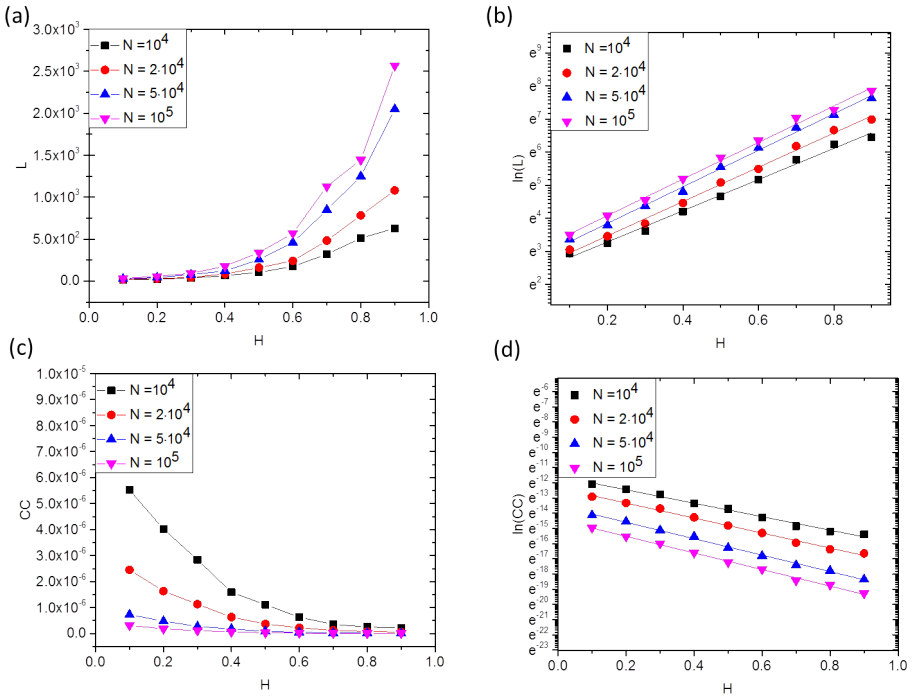

Supplementary Material, Figure S1: (a) Average path length L with different Hurst exponent values H of fBm, are presented considering a time series lengths of $N = 10^4$, $N = 2\ 10^4$, $N = 5\ 10^4$ and $N = 10^5$. (b)Average path length L in semi-logarithmic scales. It is observed that L increases exponentially in regard to $H:\ L \propto e^{bH}$,, where b increases with N. (c)Closeness centrality CC with different Hurst exponent values H of fBm, are presented considering a time series lengths $N = 10^4$, $N = 2\ 10^4$, $N = 5\ 10^4$ and $N = 10^5$.(d)Closeness centrality CC in semi-logarithmic scales. It is observed that L decreases exponentially in regard to $H:\ CC \propto e^{-bH}$, For each H, average results over 10 independent runs are shown.

S2. Characterization of fBm

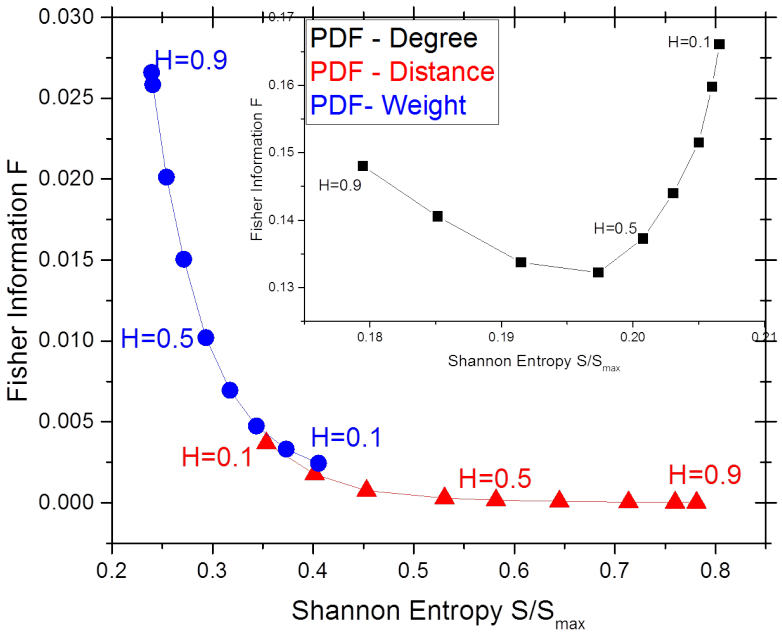

Supplementary Material, Figure S2: Shannon-and-Fisher plane for each probability density. In each case the average results for fBm with different Hurst exponent values are presented considering a time series length of 10^4 points.

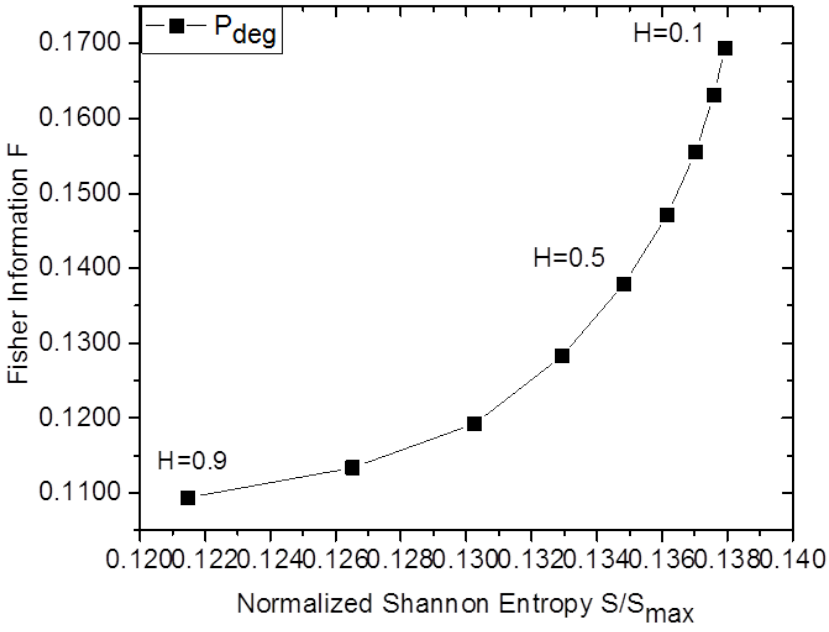

Supplementary Material, Figure S3: Shannon-Fisher plane for degree distribution. In each case the average results for fBm with different Hurst exponent values are presented considering a time series length of 10^6 points.

S3. Millennial dynamics of El Niño Southern Oscillation

Time (cal. yr BP)	P_{deg}		P_{δ}		P_w		L
	S/S_{max}	$F[P]$	S/S_{max}	$F[P]$	S/S_{max}	$F[P]$	
500	0.2664	0.1214	0.4236	0.00637	0.7046	0.045	11.5144
600	0.2657	0.1217	0.399	0.00812	0.719	0.0361	10.6906
700	0.2667	0.1216	0.3976	0.00819	0.7081	0.0422	10.5606
800	0.2688	0.1198	0.4001	0.00823	0.7022	0.045	10.3398
900	0.2655	0.141	0.4007	0.00847	0.6006	0.077	10.2456
1000	0.2671	0.1284	0.395	0.00876	0.6408	0.0679	10.1131
1100	0.2685	0.1307	0.3631	0.01362	0.6293	0.0687	9.1998
1200	0.2691	0.1466	0.3411	0.0183	0.6565	0.059	8.3263
1300	0.2699	0.1252	0.3572	0.0146	0.6527	0.0596	8.7648
1400	0.266	0.1221	0.3834	0.01085	0.6066	0.07	9.4718
1500	0.2669	0.115	0.4358	0.00694	0.5937	0.0773	11.5239
1600	0.2676	0.1138	0.4156	0.00684	0.6016	0.0759	10.8801
1700	0.2653	0.1177	0.4115	0.00719	0.5988	0.0777	10.7039
1800	0.2651	0.1171	0.4024	0.00796	0.5813	0.0829	10.4837
1900	0.2629	0.112	0.4139	0.00651	0.5304	0.0976	11.3572
2000	0.2617	0.1099	0.4144	0.00643	0.5314	0.0934	11.5213
2100	0.2592	0.1225	0.4175	0.00634	0.5333	0.086	11.4308
2200	0.2595	0.1106	0.4145	0.00645	0.5361	0.0821	11.5828
2300	0.2608	0.1261	0.4173	0.00616	0.5535	0.0799	11.7535
2400	0.2625	0.1165	0.426	0.0055	0.5702	0.0739	12.066
2500	0.2632	0.1326	0.4083	0.00699	0.6059	0.0624	11.2355
2600	0.2649	0.1327	0.4022	0.00777	0.6225	0.0554	10.7836
2700	0.2676	0.1221	0.4026	0.00786	0.6458	0.0464	10.6554
2800	0.2674	0.127	0.4182	0.00711	0.6679	0.0417	11.1384
2900	0.266	0.1426	0.418	0.00713	0.6787	0.0396	10.9759
3000	0.2681	0.1175	0.3995	0.00823	0.6889	0.0357	10.5218
3100	0.2656	0.1237	0.4447	0.00583	0.6706	0.0471	12.1715

3200	0.2629	0.1328	0.4598	0.00489	0.6206	0.0656	13.5438
3300	0.2609	0.1147	0.46	0.00424	0.6078	0.064	14.1182
3400	0.2573	0.1264	0.4567	0.00437	0.5925	0.0688	14.337
3500	0.259	0.1056	0.422	0.00586	0.5724	0.0702	12.5107
3600	0.2532	0.124	0.4216	0.00581	0.5319	0.0875	12.7108
3700	0.2529	0.1083	0.4108	0.00685	0.4941	0.1054	12.385
3800	0.2494	0.1209	0.4273	0.00533	0.4397	0.1274	12.9808
3900	0.2523	0.1085	0.431	0.00519	0.4278	0.1327	12.7609
4000	0.2515	0.1217	0.4455	0.00419	0.4362	0.1287	13.6885
4100	0.2554	0.1135	0.4522	0.00378	0.4377	0.1315	14.0459
4200	0.2586	0.1086	0.4231	0.00586	0.4779	0.1189	12.2578
4300	0.2595	0.1151	0.4212	0.00608	0.5127	0.1054	12.2266
4400	0.2617	0.1171	0.4197	0.00626	0.5549	0.0932	11.7498
4500	0.2635	0.1322	0.4336	0.00506	0.5906	0.0861	12.4412
4600	0.264	0.1194	0.4452	0.00438	0.6037	0.0756	12.8717
4700	0.2644	0.1194	0.455	0.00456	0.6145	0.0679	13.037
4800	0.2652	0.1211	0.4278	0.00587	0.6312	0.0534	11.7968
4900	0.2671	0.1131	0.398	0.00813	0.6321	0.0527	10.6825
5000	0.2642	0.1322	0.3987	0.00813	0.618	0.0605	10.5857
5100	0.2616	0.1305	0.3798	0.01048	0.6365	0.0459	10.0123
5200	0.262	0.1081	0.4008	0.00848	0.6164	0.0533	10.5102
5300	0.2611	0.1056	0.383	0.01041	0.5882	0.0683	10.032
5400	0.2594	0.1066	0.3887	0.0094	0.5332	0.0891	10.3737
5500	0.2586	0.1062	0.3837	0.01006	0.498	0.0966	10.2801
5600	0.2564	0.1164	0.4121	0.00735	0.4797	0.1079	11.2507
5700	0.2555	0.1257	0.4025	0.00769	0.4701	0.1124	11.1751
5800	0.2554	0.1157	0.415	0.00645	0.4642	0.1145	11.6628
5900	0.2565	0.1161	0.4199	0.00606	0.4643	0.1141	11.7064
6000	0.2555	0.1268	0.4173	0.00621	0.4602	0.1096	11.7947
6100	0.2581	0.1065	0.4194	0.00606	0.4403	0.1248	11.7465

6200	0.2549	0.1232	0.4249	0.00565	0.4396	0.1231	11.998
6300	0.2538	0.1269	0.4568	0.00594	0.4438	0.118	12.8527
6400	0.2575	0.1065	0.4068	0.00748	0.4533	0.1066	11.047
6500	0.2555	0.12	0.3981	0.00832	0.4324	0.1136	10.9364
6600	0.2552	0.1064	0.4194	0.00648	0.425	0.1234	11.7953
6700	0.2542	0.113	0.418	0.0062	0.4047	0.1479	11.9812
6800	0.2518	0.1157	0.4391	0.00554	0.381	0.1751	12.8768
6900	0.2489	0.1151	0.4487	0.00453	0.3549	0.2066	13.2804
7000	0.2447	0.1235	0.4967	0.00315	0.3258	0.2449	16.0753
7100	0.2444	0.1239	0.4974	0.00274	0.3048	0.2605	16.3475
7200	0.2422	0.1233	0.542	0.00203	0.2748	0.3011	20.0476
7300	0.2379	0.1223	0.5196	0.00163	0.2426	0.3357	19.5757
7400	0.2329	0.1263	0.52	0.00146	0.2162	0.379	20.471
7500	0.2301	0.1338	0.5437	0.00107	0.1984	0.4015	23.0431
7600	0.2255	0.1372	0.6251	0.00048	0.1731	0.4385	35.1152
7700	0.2238	0.1475	0.6365	0.00043	0.1704	0.4447	37.5925
7800	0.2262	0.1351	0.6284	0.00048	0.1696	0.4475	36.6095
7900	0.2252	0.131	0.6287	0.0005	0.1542	0.4721	39.0547
8000	0.224	0.1345	0.5882	0.00058	0.1664	0.4537	30.1729
8100	0.226	0.1451	0.5947	0.00058	0.1655	0.459	30.6989
8200	0.2274	0.1333	0.5792	0.0007	0.1662	0.4562	28.6701
8300	0.2271	0.1339	0.5835	0.00064	0.1456	0.4979	28.4706
8400	0.2278	0.1309	0.5647	0.00079	0.1486	0.4904	25.6507
8500	0.2256	0.1349	0.5677	0.00075	0.1345	0.5157	26.6038
8600	0.2256	0.1506	0.5763	0.00069	0.1412	0.4995	27.6848
8700	0.2296	0.1363	0.5777	0.00077	0.1452	0.4902	27.3252
8800	0.2264	0.1325	0.5539	0.0009	0.1424	0.4961	25.7429
8900	0.2265	0.1365	0.5694	0.00074	0.1364	0.5139	26.898
9000	0.2243	0.1393	0.6199	0.00042	0.1228	0.5408	35.2199
9100	0.2216	0.1388	0.5628	0.00079	0.1272	0.5424	27.1605

9200	0.2224	0.1387	0.5698	0.00073	0.1213	0.5581	27.9867
9300	0.2309	0.1298	0.5686	0.00087	0.1547	0.4716	26.0892
9400	0.2354	0.1244	0.5469	0.00123	0.1654	0.4476	23.8264
9500	0.2375	0.1333	0.543	0.00127	0.2023	0.4025	22.1613
9600	0.2434	0.1228	0.5569	0.00122	0.235	0.3517	23.5379
9700	0.2452	0.1172	0.5477	0.00127	0.2601	0.3066	21.6879
9800	0.2501	0.1121	0.5338	0.00165	0.2833	0.2667	19.6731
9900	0.2536	0.1153	0.5335	0.00197	0.3027	0.2336	19.512
10000	0.2587	0.1191	0.4827	0.00269	0.3157	0.2114	15.7687
10100	0.261	0.1145	0.4772	0.00323	0.3284	0.1848	15.1484
10200	0.2633	0.1156	0.4368	0.00482	0.3557	0.1517	13.4165
10300	0.2626	0.1201	0.4352	0.00495	0.3684	0.142	12.9306
10400	0.2629	0.1156	0.4202	0.00591	0.3791	0.1323	12.47

Supplementary Material, Table S1: Obtained quantifier values for dynamics of ENSO during the Holocene: normalized Shannon entropy value using $S[P]/S_{max}$ and Fisher information value $F[P]$; Using degree distribution, distance distribution and weights distribution,respectively. In the last column the value average path length L, is given.